CIRP Journal of Manufacturing Science and Technology 32 (2021) 120–131

Contents lists available at ScienceDirect

CIRP Journal of Manufacturing Science and Technology

journal homepage: www.elsevier.com/locate/cirpj

Emulating bistabilities in turning to devise gain tuning strategies to actively damp them using a hardware-in-the-loop simulator

G.N. Sahu[a], P. Jain[a], P. Wahi[b], M. Law[a,*]

[a] Machine Tool Dynamics Laboratory, Department of Mechanical Engineering, Indian Institute of Technology Kanpur, Kanpur 208016, India
[b] Department of Mechanical Engineering, Indian Institute of Technology Kanpur, Kanpur 208016, India

ARTICLE INFO

Article history:
Available online xxx

Keywords:
Nonlinear cutting force
Bistable
Chatter
Hardware-in-the-loop simulator
Active damping

ABSTRACT

Bistabilities in turning are characterized by the process being stable for small perturbations and unstable for larger ones. These bistabilities occur due to nonlinearities in cutting force characteristics. Characterizing these bistabilities can guide selection of cutting parameters to lie outside these zones of conditional instabilities. However, if cutting is targeted in the bistable regions, or in regions that are globally unstable, active damping methods may need to be pursued to improve the stability envelopes. Since gain tuning for active damping of chatter vibrations is usually based on linear stability analysis, it would be useful to know if those gains are adequate for damping chatter in the presence of bistabilities that occur in processes prone to strong perturbations. However, experimentation on machines to investigate these bistabilities and/or tune gains to meet targeted productivity levels with active damping is difficult due to the destructive nature of chatter. This paper hence discusses the use of a hardware-in-the-loop (HiL) simulator to emulate bistabilities and to serve as a test bench for gain tuning in the presence of bistabilities. The HiL simulator has a hardware layer comprising a flexure representing a flexible workpiece, and two actuators. One emulates the cutting force calculated in real-time in the software layer. Another serves as the active damper operating with a velocity feedback control law. Bistabilities for three different nonlinear force models are experimentally illustrated on this HiL simulator. We show that active damping can stabilize these bistable regions. Since the width of the bistable regions depend on the nonlinear force characteristics, our investigations reveal that gains must be tuned for the force model and the static chip thickness under consideration. These results are useful and can instruct active damping strategies during more realistic cutting processes with nonlinear force characteristics that exhibit conditional instabilities in the presence of strong perturbations.

Introduction

Performance of cutting processes are limited by unstable relative vibrations between the tool and the workpiece. These vibrations occur primarily because of the regeneration effect in which the vibrating tool imprints its motion on the workpiece in the form of waves being left on the surface. Succeeding revolutions may result in waves of even greater amplitudes, resulting in vibrations of increasing amplitudes [1,2]. These large amplitude vibrations damage part surface quality and may also damage elements of the machine tool system. These instabilities must hence be understood so that they can be mitigated.

Stability lobe diagrams are one convenient way to chart (in) stabilities in machining processes. The lobes establish boundaries between the stable widths/depths of cut at different speeds. If cutting takes place with parameters below these boundaries, the cut is stable. And, for cutting with parameters above these boundaries, the vibrations grow and ultimately stabilize at large, but finite amplitudes [3,4]. It has also been established that for certain cutting processes, the cut can be dynamically and conditionally stable, i.e., the cutting processes is stable for small perturbations and unstable for larger ones [4]. These bistable regions are unsafe and must be avoided. These bistabilities occur due to nonlinearities in cutting force characteristics and the extent of the bistable region around the linear stability boundary further depends on the mean uncut chip thickness [5–8].

Since there exist very many applications with possibilities of large perturbations, for example the intermittent turning of shafts with slots, and nonlinear cutting force characteristics are not unusual [7], there exists real possibilities of bistabilities occurring in practice. Characterizing these bistabilities can guide selection of cutting parameters to lie outside these zones of conditional

* Corresponding author.
E-mail address: mlaw@iitk.ac.in (M. Law).

https://doi.org/10.1016/j.cirpj.2020.11.004
1755-5817/

instabilities. However, if cutting is targeted in the bistable regions, or in regions that are globally unstable, active damping methods may need to be pursued to improve the stability envelopes. Since gain tuning for active damping of chatter vibrations is usually based on linear stability analysis, it would be useful to know if those gains are adequate for damping chatter in the presence of bistabilities that occur in processes prone to strong perturbations. However, experimentation on machines to investigate these bistabilities and/or tune gains to meet targeted productivity levels with active damping is difficult due to the destructive nature of chatter, and due to the vagaries and uncertainties in real machines.

This paper hence discusses the use of a hardware-in-the-loop (HiL) simulator to emulate bistabilities and for the HiL simulator to serve as a test bench for gain tuning for active damping in the presence of bistabilities. The HiL simulator has a hardware layer comprising a flexure representing a flexible workpiece, and two actuators. One emulates the cutting force calculated in real-time in the software layer. Another serves as the active damper operating with a direct velocity feedback (DVF) control law. Since DVF control strategies have proven to be effective [9], we limit investigations herein to only those. Learnings from experiments on the HiL simulator are expected to instruct active damping strategies during more realistic cutting processes with nonlinear force characteristics that exhibit conditional instabilities in the presence of strong perturbations.

HiL simulators offer a non-destructive, cost-effective, repeatable, and safe platform for investigations. As such, they have been used to also study chatter. Amongst the first to do so were Ganguli et al. [10,11] who studied chatter in turning and milling using a HiL simulator. HiL simulators have also been used as a test bench to investigate different active vibration control strategies to mitigate chatter [10–14], and some of these learnings have also been transferred to actively control vibrations in real machining processes [15]. Since the HiL simulator must correctly represent the physics of the interaction of the process with the machine tool system, and since HiL simulators have actuators and measurement transducers, and involve signal conditioning and real-time computation, sometimes the emulated behavior is different than model predictions. Since delays in the HiL simulator cause this difference, research has also systematically characterized such delays and proposed ways to mitigate them [13,14]. Other impressive research on the use of HiL simulators has used non-contact methods of excitation to correctly account for dynamics of rotating systems potentially changing with speeds [16–18]. Recent research has also characterized the unexpected nonlinearities of the contactless actuators [19] to investigate why emulated behavior deviates from predictions.

Although previous uses of a HiL simulator to investigate chatter and test active damping strategies have proved effective, those investigations have mostly been restricted to processes with linear cutting force characteristics. And, though some recent work emulated a nonlinear force model in the HiL simulator [18] or discussed the influence of nonlinear force characteristics on finite amplitude instabilities [20], there are no reports of investigations on emulating bistabilities in HiL simulators. Nor are there any reports on active vibration control in the presence of nonlinearities in the cutting process resulting in bistable behavior. Since we discuss the use of a HiL simulator to emulate bistabilities in turning and investigate if tuning strategies for active vibration control in the presence of such instabilities need to be different, all such analysis presented herein is new.

The remainder of the paper is organized as follows. At first, a simple mechanical model of a flexible workpiece being excited by cutting forces with nonlinear characteristics is introduced. The nonlinear cutting force models are based on the established work of others. We investigate the power-law model [21], the cubic

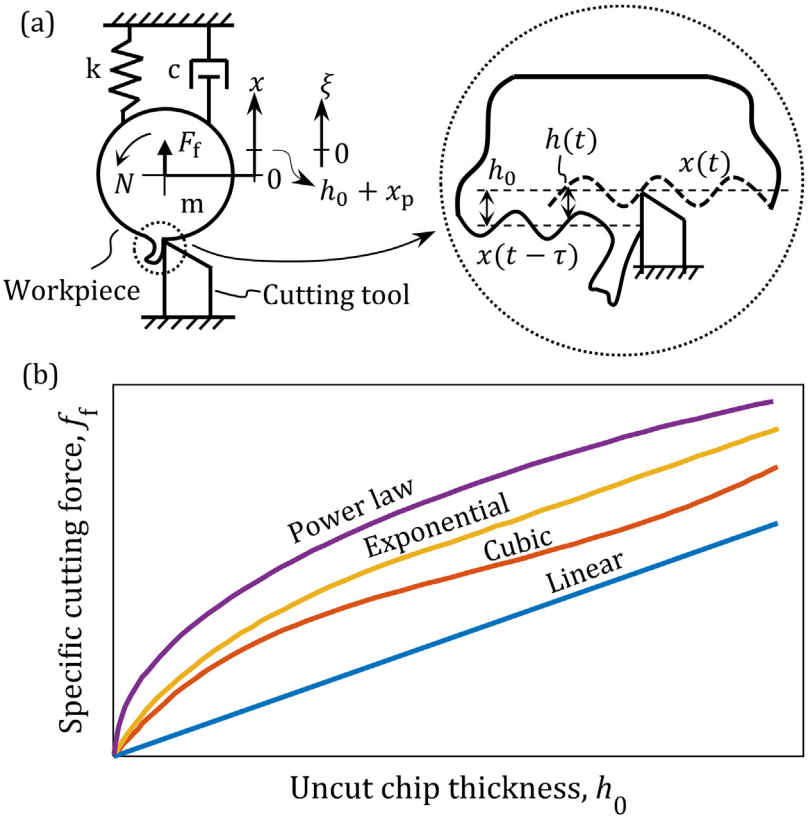

Fig. 1. (a) Mechanical model of turning tool-workpiece interaction, (b) Schematic representation of cutting force characteristics of interest.

polynomial force characteristics [4], and the exponential force model [22]. To solve for stability using the established semi-discretization method [23], we linearize the force models using a Taylor series approximation about the mean chip thickness. Bistable regions are obtained by the analytical formulae given in Ref. [8].

The third main section describes the main elements of the HiL simulator — which builds on our earlier reported work [14,20]. Since the simulator is validated, we focus here only on the key differentiating elements. We discuss the use of a surface location storage (SLS) algorithm to incorporate the multiple regenerative effects to account for the tool leaving the cut nonlinearity to emulate finite amplitude instabilities along the lines of Refs. [24–27]. This improves the behavior of the overall HiL simulator from the previously used transport delay block in Ref. [14]. Since the setup has two actuators, one to emulate the cutting force, and another for active damping, and since both have different characteristics, we briefly discuss methods to compensate for their behavior. Finally, in the software layer, we employ a forward Euler-based numerical integration scheme to obtain displacements for the estimation of the total chip thickness.

The fourth main section discusses emulation of bistabilities for the three different nonlinear force characteristics of interest. Stability analysis is followed by demonstrating how active damping can stabilize these bistable regions. Since the width of the bistable regions depends on the static chip thickness and the nonlinear force characteristics, we also show that gains must be tuned for the force model and the static chip thickness under consideration. This is followed by the main conclusions of the paper.

Mechanical model with cutting process nonlinearities

The mechanical model of the turning process is shown in Fig. 1(a). We assume the tool is rigid, and that the workpiece is flexible only in the feed direction, and that it can be approximated as a single degree of freedom system. The governing equation of motion for the tool interacting with the workpiece is:

$$\ddot{x}(t) + 2\zeta\omega_n\dot{x}(t) + \omega_n^2 x(t) = \frac{F_f(t)}{m} \tag{1}$$

wherein m is the modal mass (kg), ζ the damping ratio, and ω_n the natural frequency (rad/s). The cutting force, $F_f(t)$ is characterized by a coefficient, a depth of cut (b), and the chip thickness ($h(t)$).

The cutting force can be more generally expressed as a product of the depth of cut and a specific cutting force (f_f), i.e., $F_f(t) = bf_f(t)$, wherein the form of f_f describes the force being linear or not. If assumed linear, the usual form of the cutting force for the case of ploughing effects being ignored is:

$$f_f^L(t) = K_{fh}(t), \tag{2}$$

wherein K_f is an empirically determined coefficient which depends on the material being cut, the geometry of the tool, and on the cutting parameters. If, however, the cutting force is nonlinear, it can take many forms. Established forms for such nonlinearities of interest herein are the power-law form [21], the cubic form [4], and the exponential form [22]. If assumed to be of the power-law form, the force is:

$$f_f^P(t) = K_{fp}h(t)^\nu, \tag{3}$$

wherein K_{fp} is again an empirically determined coefficient, and ν is a cutting force exponent, usually taken to be 3/4 [21]. If on the other hand, the force takes a cubic form, it becomes:

$$f_f^C(t) = \rho_1 h(t) + \rho_2 h^2(t) + \rho_3 h^3(t), \tag{4}$$

wherein $\rho_{1,2,3}$ are also empirical coefficients obtained from the cutting experiments [4]. Finally, if the force takes the exponential form, it becomes:

$$f_f^E(t) = b_1 h(t) + \frac{b_2}{b_3} e^{b_3 h(t)} + b_4, \tag{5}$$

wherein $b_{1,2,3,4}$, like the other constants, are also empirically determined [22]. Above four forms for the cutting force characteristics are shown schematically in Fig. 1(b).

The force, regardless of its form, excites the system. The system responds, i.e., it vibrates and changes the nature of the force in turn, which again excites the system. This interaction, described as the regenerative effect, results in a dynamically varying chip thickness, $h(t)$, which depends on the mean chip thickness (h_0), the vibrations of the current revolution $x(t)$ and of the previous revolution $x(t-\tau)$, and can be described by: $h(t) = h_0 - x(t) + x(t-\tau)$, wherein τ is spindle period in seconds, also called the regenerative delay, which is evaluated by $\tau = 60/N$, wherein N is the spindle speed. For large amplitude vibrations, the cutting tool may lose contact with the workpiece, resulting in the force instantaneously becoming zero, i.e., $F_f(t) = 0$ when $h(t) \leq 0$. This results in finite amplitude instabilities. The tool being out of cut condition also results in multiple regenerative effects. And, in such cases, the chip thickness is estimated as $h(t) = x_{min} - x(t)$, wherein, x_{min} is the smallest value of $\{h_0 + x(t-\tau), 2h_0 + x(t-2\tau), \ldots\}$ taken over several previous revolutions. These conditions are implemented within the HiL simulator using an elegant surface location storage algorithm that overcomes the need to store and track the different time-delays.

The linear force when substituted in Eq. (1) results in a linear delay differential equation (DDE), whereas when any of the nonlinear force characteristics from Eqs. (3), (4), or (5) are substituted in Eq. (1), the resulting equation is a nonlinear DDE. These nonlinear equations can be solved using generalized time domain numerical integration schemes [3]. However, since these numerical schemes are computationally inefficient, the nonlinear equations can be linearized using a Taylor series expansion to solve for stability boundaries in the frequency domain [28], or by using other established time-efficient semi-discretization methods (SDM) [23]. Since the SDM method is well-equipped to handle nonlinearities by linearizing them, we prefer to use it for all theoretical analysis herein.

Linearization of the nonlinear delay differential equations

We linearize based on the methods proposed in Ref. [29]. We assume that the flexible workpiece has a motion of the form $x(t) = h_0 + x_p(t) + \xi(t)$, in which $x_p(t) = x_p(t+\tau)$ is the amplitude of vibration when there is no regenerative chatter (i.e., the forced vibration amplitude), and $\xi(t)$ is the amplitude of vibration after any perturbation, see Fig. 1(a).

Considering the case of the nonlinear force characteristics being of the form of the power-law, and substituting the assumed motion ($x(t)$) in a modified form of Eq. (1), with the force being $F_f(t) = bf_f^P(t)$, the modified equation of motion becomes:

$$\ddot{x}_p(t) + 2\zeta\omega_n\dot{x}_p(t) + \omega_n^2 x_p(t) + \ddot{\xi}(t) + 2\zeta\omega_n\dot{\xi}(t) + \omega_n^2\xi(t) = \frac{K_{fp}b}{m}(h_0 + \xi(t-\tau) - \xi(t))^\nu. \tag{6}$$

The nonlinear term on the right-hand side is linearized about the specified uncut chip thickness, h_0 using a Taylor series expansion. Ignoring the higher order terms, the linearized form of

Eq. (6) becomes:

$$\ddot{x}_p(t) + 2\zeta\omega_n\dot{x}_p(t) + \omega_n^2 x_p(t) + \ddot{\xi}(t) + 2\zeta\omega_n\dot{\xi}(t) + \omega_n^2\xi(t) = \frac{K_{fp}b}{m}h_0{}^{\nu} + \frac{K_{fp}b\nu(h_0)^{\nu-1}}{m}(\xi(t-\tau) - \xi(t)). \quad (7)$$

For the case of there being no regenerative chatter, $\xi(t) \equiv 0$, and Eq. (7) reduces to:

$$\ddot{x_p}(t) + 2\zeta\omega_n x_p(t) + \omega_n^2 x_p(t) = \frac{K_{fp}b}{m}(h_0)^{\nu}. \quad (8)$$

From Eqs. (7) and (8), the linear DDE in ξ becomes:

$$\ddot{\xi}(t) + 2\zeta\omega_n\dot{\xi}(t) + \omega_n^2\xi(t) = \frac{b}{m}K_{fp}\nu(h_0)^{\nu-1}(\xi(t-\tau) - \xi(t)). \quad (9)$$

Using the same approach as above, the linear DDEs for the cubic force model can be shown to be:

$$\ddot{\xi}(t) + 2\zeta\omega_n\dot{\xi}(t) + \omega_n^2\xi(t) = \frac{b}{m}\left(\rho_1 + 2\rho_2 h_0 + 3\rho_3 {h_0}^2\right)(\xi(t-\tau) - \xi(t)). \quad (10)$$

Similarly, for the exponential force model, the linear DDE becomes:

$$\ddot{\xi}(t) + 2\zeta\omega_n\dot{\xi}(t) + \omega_n^2\xi(t) = \frac{b}{m}\left(b_1 + \frac{b_2}{b_3}\left(1 + \sum_{n=1}^{N_T}\frac{(b_3)^n n(h_0)^{n-1}}{n!}\right) + b_4\right)(\xi(t-\tau) - \xi(t)), \quad (11)$$

wherein N_T is the number of terms in the Taylor series to sufficiently linearize the exponent.

Check for stability using the semi-discretization method

Theoretical checks for stability are performed using the semi-discretization method [23]. This requires the linearized DDEs to be first converted to a state space form as follows:

$$\dot{\boldsymbol{\xi}}(t) = \mathbf{A}(t)\boldsymbol{\xi}(t) + \mathbf{B}(t)\boldsymbol{\xi}(t-\tau), \quad (12)$$

wherein $\mathbf{A}(t) = \begin{bmatrix} 0 & 1 \\ -\left(\omega_n^2 + \frac{F_f}{m}\right) & -2\zeta\omega_n \end{bmatrix}$, $\mathbf{B}(t) = \begin{bmatrix} 0 & 0 \\ \frac{F_f}{m} & 0 \end{bmatrix}$, and F_f could take on any of the linear and/or linearized forms of the nonlinear force characteristics.

The next step is to divide the delay (time) period into k discrete time intervals $\Delta t\,(\in [t_i,\ t_{i+1}]$ of length $\Delta t, i = 0, 1, 2, \ldots)$, such that $T = k\Delta t$. Delayed positions are approximated using the weighted sum of two nearest delayed positions in a discrete map as $\boldsymbol{\xi}(t-\tau) \approx \boldsymbol{\xi}(t_i + \Delta t/2 - \tau) \approx w_b\boldsymbol{\xi}_{i-k} + w_a\boldsymbol{\xi}_{i-k+1}$ wherein w_a and w_b are weight functions, both being 1/2 for turning processes.

The solution of Eq. (12) is:

$$\boldsymbol{\xi}_{i+1} = \mathbf{P}_i\boldsymbol{\xi}_i + w_a\mathbf{R}_i\boldsymbol{\xi}_{i-k+1} + w_b\mathbf{R}_i\boldsymbol{\xi}_{i-k}, \quad (13)$$

wherein $\mathbf{P}_i = \exp(\mathbf{A}_i\Delta t)$ and $\mathbf{R}_i = (\exp(\mathbf{A}_i\Delta t) - \mathbf{I})\mathbf{A}_i^{-1}\mathbf{B}_i$, and $\mathbf{I}$ is an identity matrix, and $\mathbf{A}_i = \frac{1}{\Delta t}\int_{t_i}^{t_{i+1}}\mathbf{A}(t)\mathrm{d}t$, and $\mathbf{B}_i = \frac{1}{\Delta t}\int_{t_i}^{t_{i+1}}\mathbf{B}(t)\mathrm{d}t$, respectively. Following Eq. (13), a discrete map can be defined as $\boldsymbol{\chi}_{i+1} = \mathbf{C}_i\boldsymbol{\xi}_i$, wherein $\mathbf{C}_i$ is the coefficient matrix, and $\boldsymbol{\xi}_i = \mathrm{col}(\boldsymbol{\xi}_i,\ \boldsymbol{\xi}_{i-1}, \ldots\ \boldsymbol{\xi}_{i-k})$.

The next step is to determine a transition matrix $\boldsymbol{\varphi}$, which connects $\boldsymbol{\chi}_0$ and $\boldsymbol{\chi}_k$, such that $\boldsymbol{\chi}_k = \boldsymbol{\varphi}\boldsymbol{\chi}_0$, wherein $\boldsymbol{\varphi} = \mathbf{C}_{k-1}\mathbf{C}_{k-2}\ldots\mathbf{C}_1\mathbf{C}_0$. Stability investigations, hence, reduce to finding the eigenvalues of $\boldsymbol{\varphi}$. If the modulus of eigenvalues of $\boldsymbol{\varphi} < 1$, then the system is asymptotically stable. Stability lobe diagrams are generated by scanning the depths of cut for every speed within the speed range of interest. The depths at which the modulus of eigenvalues of $\boldsymbol{\varphi} = 1$ correspond to the limit of stability and establish the boundaries (lobes). These boundaries correspond to the global unstable limits.

Estimating bistable regions

Cutting in the bistable region is conditionally stable and depends on the level of perturbations. Knowledge of the width of these regions is useful to avoid them and/or to design active damping strategies to ensure that cutting in these regions is stable. Since the global unstable limit has already been established by solving the linearized DDEs, the width of the bistable regions is estimated herein based on the closed-form analytical expressions derived by Molnar et al. in Ref. [8].

As per Ref. [8], if the magnitude of the bistable region is R_{bist}, and if the global unstable limit is b_{lim}, then the global stable limit of bistable region (b_{bist}) can be evaluated as:

$$b_{bist} = (1 - R_{bist})b_{lim}. \quad (14)$$

For the power-law form of the nonlinearity, the expression for R_{bist} is:

$$R_{bist}^{P} = 1 - \frac{\sqrt{\pi}\,\Gamma(\nu+2)}{2^{\nu+1}\,\Gamma\left(\nu+\frac{1}{2}\right)}, \quad (15)$$

wherein Γ is the Euler gamma function. For the cubic form of the cutting force characteristics, the size of the bistable region is:

$$R_{bist}^{C} = \frac{3\rho_3 h_0^2}{4\rho_1 + 8\rho_2 h_0 + 15\rho_3 h_0^2}, \quad (16)$$

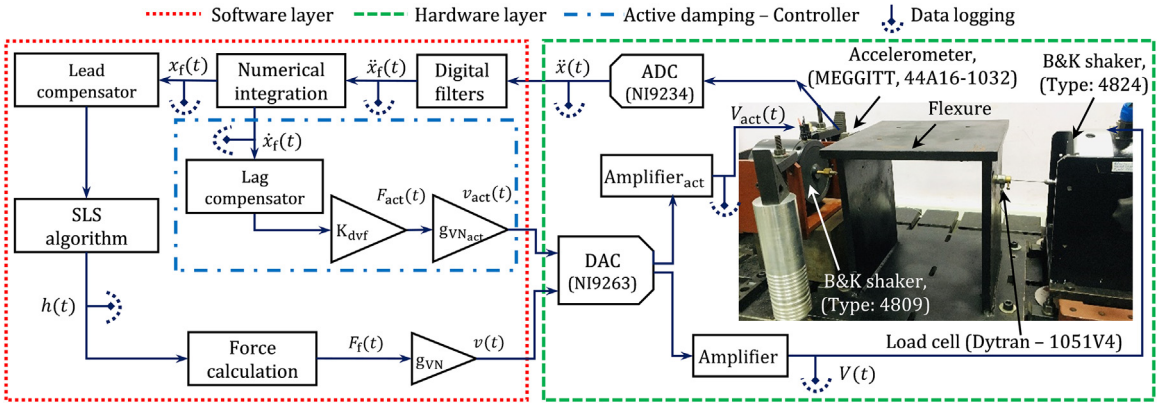

Fig. 2. Hardware and software layers of the HiL simulator integrated with an active damping system.

wherein $\rho_{1,2,3}$ are the same empirically determined coefficients as those listed in Eq. (4).

In the case of the exponential force characteristics, the expression for the size of the bistable region is:

$$R^{E}_{bist} = 1 - \frac{b_1 h_0 + b_2 h_0 e^{b_3 h_0}}{b_1 h_0 + 2\frac{b_2}{b_3} e^{b_3 h_0} I_1(b_3 h_0)}, \quad (17)$$

where I_1 is the modified Bessel function of first kind, and $b_{1,2,3,4}$ are the same as those listed in Eq. (5).

Having outlined the mechanical model with nonlinear force characteristics, and having linearized the resulting DDEs, and having discussed methods to solve for stability and to identify the bistabilities, we now describe the HiL simulator and subsequently emulate bistabilities on it.

Hardware-in-the-loop (HiL) simulator

The HiL simulator consists of a hardware and a software layer as shown in Fig. 2. These layers interact with each other in a closed-loop sense to represent the closed-loop interaction between a tool and a flexible workpiece. Since this HiL simulator was already validated in Ref. [14], we only describe the key differentiators between this setup and that in Ref. [14].

The hardware layer

The hardware layer consists of two shakers, each with its own power amplifier. The hardware layer also consists of an analog to digital converter (ADC) and a digital to analog converter (DAC). The main shaker (type 4824, force capacity of 100 N) operates in the DC voltage mode and applies the emulated cutting force on the flexure. The secondary shaker (type 4809, force capacity of 45 N) operates in its AC voltage mode and applies the force for active damping. Unlike other HiL simulator setups [13] in which the shakers are hung to minimize chances of its membranes being preloaded due to fixed boundary conditions, we fix shakers on a rigid table. And, based on our prior work [14], we select stingers carefully such that the shaker's boundary conditions and/or its moving mass does not significantly alter the flexure's response. We excite the flexure at a flexible point such that the force needed to result in large amplitude motion is not large. Attachment of the active damper is also chosen at a location with large amplitudes of motion such that the active damping force requirement also remains modest. Both shakers were operated such as to not saturate them in current and/or in stroke.

The flexure's dynamics are evaluated using the main shaker. A sinusoidal chirp signal between 30 Hz and 900 Hz is supplied to the shaker in an open-loop configuration. The load applied is measured using a load cell, and the response of the flexure to the excitation is measured using an accelerometer. The flexure was observed to behave like a single degree of freedom system approximating a flexible workpiece, with modal parameters evaluated to be $m = 15.5\,kg$, $k = 8.5 \times 10^6$ N/m, $\zeta = 0.26\,\%$, and $f_n = 118$ Hz. F/V characteristics (magnitude and phase) of both shakers were evaluated as detailed in Ref. [14]. From the magnitudes, we estimated a gain (g_{VN}) of 0.075 V/N for the primary shaker, and a gain ($g_{VN_{act}}$) of 0.036 V/N for the secondary shaker. Phase characteristics of both shakers were used to estimate a delay attributable to each of these. Suspension frequencies of the main and secondary shakers were estimated to be 21 Hz and 71 Hz, respectively. Since these are far apart enough from each other, and from the flexural mode, they do not interfere with each other and/or the flexure.

The software layer

The software layer consists of data acquisition and signal processing, i.e., filtering, real-time computations to calculate the regenerative cutting force and the active damping force and includes data logging for post-processing. The software layer is implemented in a LabVIEW environment using a controllable NI cRIO-9040 module with an onboard Field Programmable Gate Array (FPGA) module. The software layer acquires and processes all data at the rate of 5 kHz. To filter the high-frequency noise, we apply a second-order low pass filter with a cut off frequency of 700 Hz. And to also filter the low-frequency suspension mode of the main shaker, we also apply a first-order high pass filter with a cut off frequency of 40 Hz. Since these filters alter the measured accelerations, gain and phase characteristics of these were evaluated as outlined in Ref. [14] to be suitably compensated.

To obtain displacements and velocities from the measured accelerations, and to establish stability, we implement an efficient and simple forward Euler numerical integration scheme within LabVIEW. The numerical integration method used herein is found to be quicker than the hardware integrator that was previously used in Ref. [14]. The step size for integration is taken to be 0.2 ms. Since this is significantly smaller than the period of ~8.5 ms corresponding to the mode of the flexure, no numerical stability issues are expected with the use of this scheme.

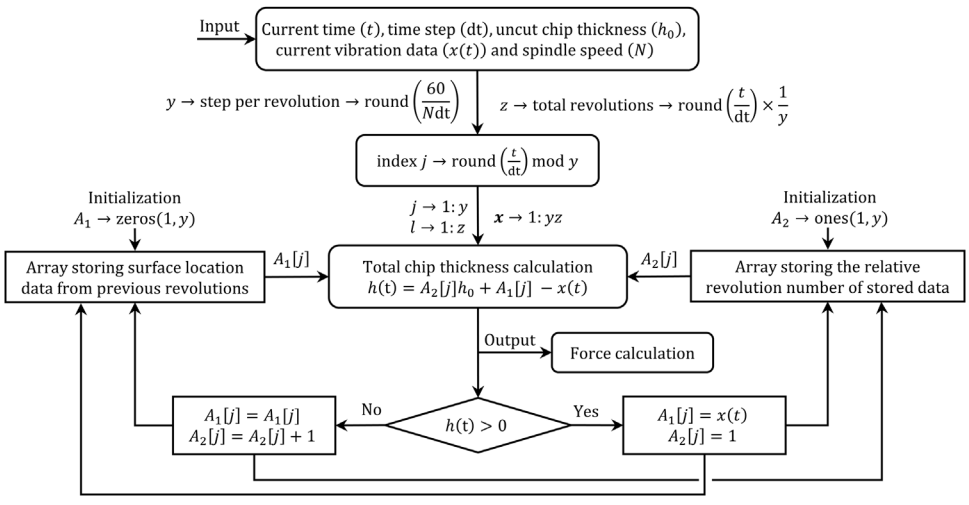

Fig. 3. Surface location storage (SLS) algorithm for calculating the total chip thickness.

The software layer also includes implementation of a surface location storage (SLS) algorithm for the estimation of the total chip thickness along the lines of Refs. [24–27]. The SLS algorithm accounts for finite amplitude instabilities, i.e., the basic nonlinearity that occurs when the amplitudes of vibrations are sufficiently large for the tool to leave the cut. The dependency of the total chip thickness ($h(t)$) on the resulting multiple regenerative effects requires storing data from all previous revolutions. In the SLS algorithm, instead of storing the displacement data from the previous revolutions, we store only the profile of the surface to be cut by the tool in the current revolution. This cut surface profile incorporates all the necessary information about the displacement of the tool from all previous revolutions. The flowchart of the SLS algorithm is outlined in Fig. 3.

The traditional method to estimate $h(t)$ uses the entire history of the displacement response $x(t)$ stored in the vector $\boldsymbol{x}$ to emulate possible multiple regenerative effects during cutting [3]. Accordingly, if the integration step-size is chosen such that there are y number of displacement responses per revolution, the length of the vector $\boldsymbol{x}$ increases as time progresses. Because of the limited size of storage space available, practical implementation focuses only on a finite number of revolutions. If the total number of revolutions under consideration is z, the size of the vector $\boldsymbol{x}$ which must be stored becomes yz. This could become prohibitively large when the cutting conditions are such that the number y is large and z is also required to be large from the numerical accuracy point of view. To circumvent this issue, we account for the multiple regenerative effects by only storing the current cut surface data using two arrays A_1 and A_2, both of lengths governed by the number of discrete steps considered in a revolution (y). Array A_1 stores the relative vibrations between the tool and the workpiece as marked on the current surface and is initialized with '0' for the first revolution ($l = 1$) which implies that we are starting with a flat uncut surface. Hence the entries in the array A_1 basically represent the profile of the immediate surface (over one revolution) that is approaching the cut in a discretized form. The array A_2 stores the previous revolution number whose relative vibration data is reflected in the cut surface and is initialized with '1' for the first revolution thereby specifying that in the first revolution, vibration from only the previous revolution is marked on the cut surface throughout its angular extent, see Fig. 3. This information about the previous revolution number whose vibration is imprinted on the surface is required to calculate the total chip thickness.

The total chip thickness, $h(t)$ is, hence, calculated using the stored data in the arrays A_1 and A_2 for the corresponding index of the current angular location using the equation given in Fig. 3. This calculated chip thickness is used further to check if the tool is in cut or not at this location, and the data in the arrays are updated accordingly for the next revolution ($l + 1$). If the tool is in cut at an angular location indexed by j, i.e., if $h(t) > 0$, data stored in arrays A_1 and A_2 at index j is updated with the current revolution data ($x(t)$) and '1', respectively. However, if the tool is not in cut, i.e., if $h(t) \leq 0$, the data stored at $A_1[j]$ remains unchanged, but the relative revolution number stored in $A_2[j]$ is increased by 1.

Instead of using two arrays, alternatively, one could have used a single array A_1 whose entry at index j is updated with the current revolution data ($x(t)$) if $h(t) > 0$, while incrementing the entry at index j of the array A_1 by h_0 if $h(t) \leq 0$. This would eliminate the need for the second array A_2, as was suggested in Ref. [31]. However, numerical analysis and experiments on the HiL simulator show that the use of a single array does not influence the computational time. And since the second array A_2 tracks how the cut surface depends on the previous revolution numbers, it also provides a sense of severity of the multiple regenerative effects, and hence we retain the two array implementation.

Though the use of the SLS algorithm to estimate $h(t)$ was expected to be computationally more efficient than the traditional method based on estimating $h(t)$ from stored data from previous revolutions, a check for a representative case of $h(t)$ being potentially dependent on three previous revolutions' displacement data shows the SLS algorithm to offer no computational advantage over the traditional method. However, since the SLS algorithm allows for a more generalized estimation of $h(t)$ being dependent on the displacement data of any number of previous revolutions (periods), we retain its use for all analysis herein.

Displacements once estimated are used to estimate the total chip thickness, which in turn is used in conjunction with the force model of interest. The calculated forces, converted to voltage signals, are then transferred to the main shaker through its power amplifier using the DAC. The software layer also includes the control block for active vibration control operating with a velocity feedback control law. The damping forces are also converted to voltage signals and are then transferred to the secondary shaker through its power amplifier using the same DAC.

Compensating delay in the HiL simulator

Each of the hardware and software elements of the simulator have their characteristic behavior and delay. This results in the emulated behavior on the HiL simulator differing from theoretical predictions. To address this, delay in all elements are estimated as outlined in [14]. For the regenerative loop, the total delay, τ_{delay} in the HiL simulator was estimated to be ~0.8 ms. This is less than the delay of ~1.5 ms reported in Ref. [14]. This delay in the regenerative loop is compensated using a phase lead compensator. The total phase to be compensated is estimated as $\theta_{\text{comp-lag}} = (\tau_{\text{delay}} \times \omega_{\text{n}})180/\pi \cong -33.96^{\text{o}}$. The compensator is designed based on recommendations in Ref. [13,14]:

$$C_{\text{lead}}(s) = \frac{\mathrm{K}_1\left(\left(\frac{s}{\mathrm{z}_1}\right)^2 + 2\zeta_{\text{c}}\left(\frac{s}{\mathrm{z}_1}\right) + 1\right)}{(s+\mathrm{p}_1)(s+\mathrm{p}_2)(s+\mathrm{p}_3)}, \tag{18}$$

wherein $\mathrm{K}_1 = 8.072 \times 10^8$, $\mathrm{z}_1 = 253.61$ rad/s, $\zeta_{\text{c}} = 2.04$, $\mathrm{p}_1 = 375.27$ rad/s, $\mathrm{p}_2 = 5525.8$ rad/s, and $\mathrm{p}_3 = 2345.9$ rad/s, respectively. And, though the compensator in Eq. (18) has the same structure as in Ref. [14], its coefficients are different due to the delay being different.

For the active damping loop, we separately characterized the delays on account of the secondary shaker, the digital filter, and the numerical integration scheme. The resulting phase estimated at the natural frequency of the flexure is positive due to the large phase lead contributed by the digital filter and only a small delay due to the secondary shaker. The phase of $\theta_{\text{comp-lead}} = 24.62^{\text{o}}$ is compensated using a standard first-order phase lag filter defined as:

$$C_{\text{lag}}(s) = \frac{s + \frac{1}{\mathrm{aT}}}{s + \frac{1}{\mathrm{T}}} \equiv \frac{s + \frac{1}{0.412(2\pi \times 0.00042)}}{s + \frac{1}{2\pi \times 0.00042}}, \tag{19}$$

wherein $\mathrm{a} = (1 - \sin(\theta_{\text{comp-lead}}))/(1 + \sin(\theta_{\text{comp-lead}}))$, and 1/T is the pole of $C_{\text{lag}}(s)$. This is tuned to get the desired phase at the natural frequency of the flexure while ensuring that the phase lag reduces as the frequency increases. Since this compensator results in a gain of 3.13 dB, the velocity signal is corrected by multiplying it with the factor of 1/3.13 dB.

Emulating bistabilities using the HiL simulator

Bistable behavior was emulated on the HiL simulator to characterize its dependence on the form of the force model as

well as to establish its dependence on the mean chip thickness. Separate experiments were undertaken for the linear force model and for each of the three nonlinear force models. To investigate stability, the flexure was initially perturbed by applying a static force on it. The virtual depth of cut (b) was then increased in steps of 5 μm at a specified virtual spindle speed (N) and the response was monitored to detect if the system is stable or not. In the case of a stable depth of cut, the flexure responds to the initial perturbation, and then the transients slowly die down. However, for the case of an unstable depth of cut, due to regenerative effects after the initial perturbation, the response $x(t)$ starts to grow with time and saturates at finite amplitudes of displacements and forces. The critical depth of cut and the corresponding observed oscillation frequency (chatter frequency) for that case is recorded. These stability conditions correspond to the global unstable limits.

For finding the global stable limits, i.e., to find the lower limits of the bistable regions, for every speed of interest, the depths of cuts were decreased in the same step size as they were increased with to find the global unstable limit. And the last but one depth of cut at which the finite amplitude instabilities disappear, i.e., the depth of cuts just before which the tool is always in contact with the workpiece and the cut is stable is recorded as the lower limit of the bistable region. The change in the depth of cut is a perturbation, and hence this method of finding the limit of the bistable region is thought to be valid.

Representative experimental observations for a stable and an unstable case for emulated behavior for the exponential force model for the case of the static chip thickness being 15 μm are shown in Fig. 4. The change in the force and displacement characteristics for the stable and unstable case are evident in Fig. 4. For the stable case, even though the voltage output from the amplifier shows the DC component, since the load cell and the accelerometer cannot measure DC components, their signals respond to the initial perturbation, decay, and then oscillate about a mean of zero. Similarly, for the unstable case, even though the voltage output from the amplifier shows that the voltage supplied to the shaker oscillates about a non-zero mean, and that it reaches zero at instants for when the tool leaves the cut, the same behavior is not evident in the measured force signals, which record a negative force when the force should have been zero. This artefact is artificial and is limited by the working principle of the load cell and is not a characteristic of the system. Despite this, the force, and

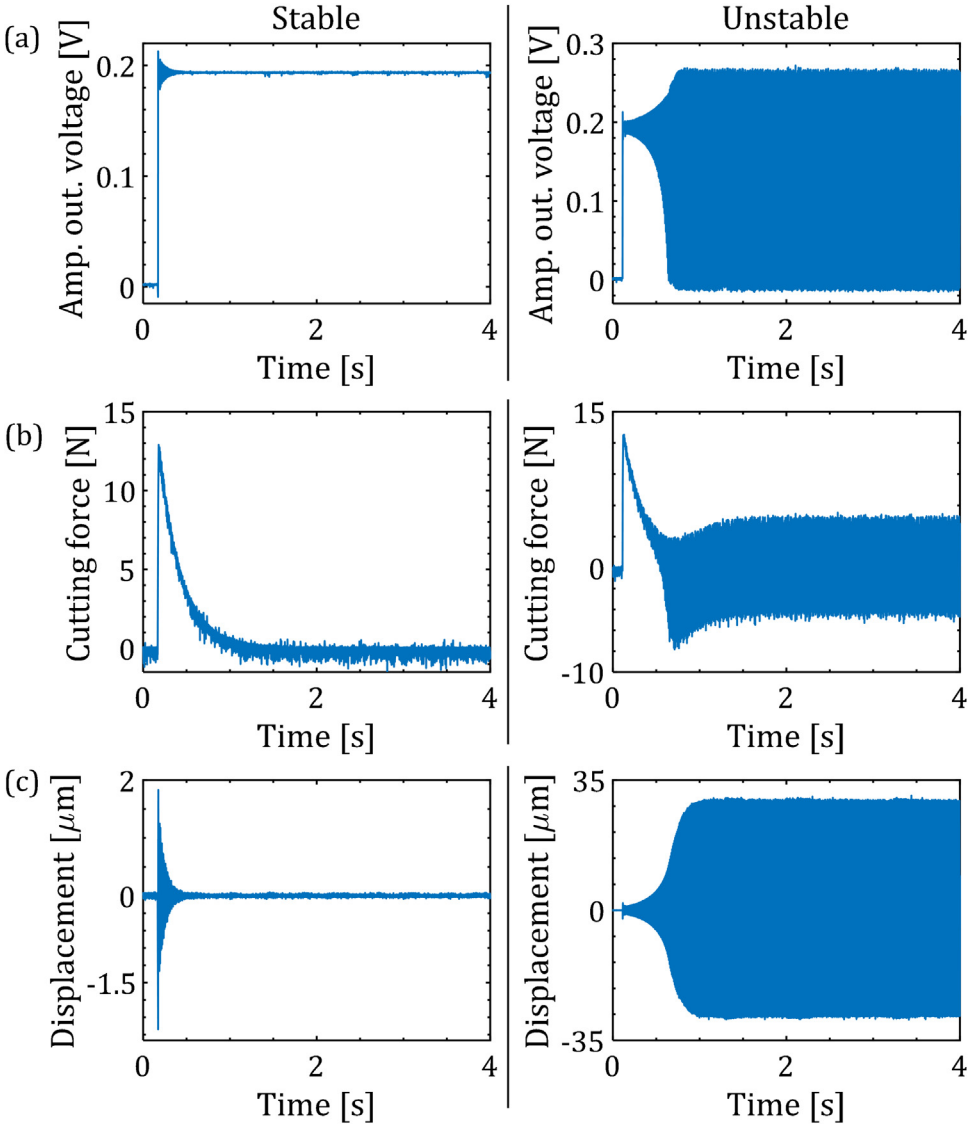

Fig. 4. Representative experimental cases with exponential force model, $h_0 = 15\,\mu$m, showing stable ($b = 0.15$ mm, $N = 3000$ rpm) and unstable behavior ($b = 0.15$ mm, $N = 2600$ rpm). (a) Voltage output from the amplifier, (b) Measured forces, (c) Recorded displacements.

displacements exhibit expected characteristics of finite amplitude instabilities.

To ease identification of (un)stable limits on the HiL simulator the procedure was automated. The stability criterion was defined as that at which for given parameters, the cutting force becomes zero due to the tool jumping out of cut. A check for force becoming zero was done using a standard *if* and *else* condition within the software layer. And, since the load cell that we used cannot properly record the force dropping to zero for the condition of the tool leaving the cut, we instead use the emulated force signal within the software layer that is supplied to the shaker's amplifier to detect if the cut is stable or not. Using this routine, experimental characterization as shown in Fig. 4, was repeated for every selected virtual spindle speed in the range of 1800 rpm–3000 rpm for every force model of interest, and the resulting stability boundaries are shown in Fig. 5. All emulated results shown in Fig. 5 are for the delay in the HiL simulator being compensated. Results in Fig. 5 include comparisons with theoretical predictions that are obtained by using the semi-discretization method.

For the nonlinear force models, theoretical global unstable results were obtained by solving the linearized form of the DDEs (Eqs. (9)–(11)) using the semi-discretization method. To linearize the exponential force model, the number of terms in the Taylor series was selected to be 25 – based on a convergence analysis, i.e., in Eq. (11), $N_T = 25$. To solve for stability using the SDM, for the linear force model, the power-law model, and the cubic force models, each period (revolution) was discretized in 100 steps, i.e., $k = 100$, and for the exponential force model, results were found to converge for $k = 250$. For the nonlinear force models, theoretical global stable limits shown in Fig. 5 were obtained from Eqs. (14)–(17).

To obtain results shown in Fig. 5, for the linear force model, the cutting coefficient was taken to be $K_f = 1384\ \mathrm{N/mm^2}$ [14]. For the power-law form of the force model, the cutting coefficient K_{fp} is taken to be $1384\ \mathrm{N/mm^{\nu}}$, wherein ν is taken to be 3/4 [21]. For the case of the cubic polynomial force model, the coefficients are taken from reports in Ref. [4], i.e., $\rho_1 = 6109.6\ \mathrm{N/mm^2}$, $\rho_2 = -54141.6\ \mathrm{N/mm^3}$, and $\rho_3 = 203769\ \mathrm{N/mm^4}$. And, for the exponential form of the force model, the coefficients are taken from reports in Ref. [30], i.e., $b_1 = 176\ \mathrm{N/mm^2}$, $b_2 = 4386\ \mathrm{N/mm^2}$, $b_3 = -129\ \mathrm{mm^{-1}}$, and $b_4 = 34\ \mathrm{N/mm}$. For each force model type, four different levels of the uncut chip thickness are analysed. The four levels are: $5\,\mu$m, $10\,\mu$m, $15\,\mu$m and $20\,\mu$m. These levels are selected such that for emulations on the HiL simulator, the main shaker does not saturate in force.

As is evident from Fig. 5, in which experimental markers are overlaid on the theoretical continuous curves, emulated results on the HiL simulator agree very well with theoretical predictions. We emphasize here that the globally unstable limits for the theoretical

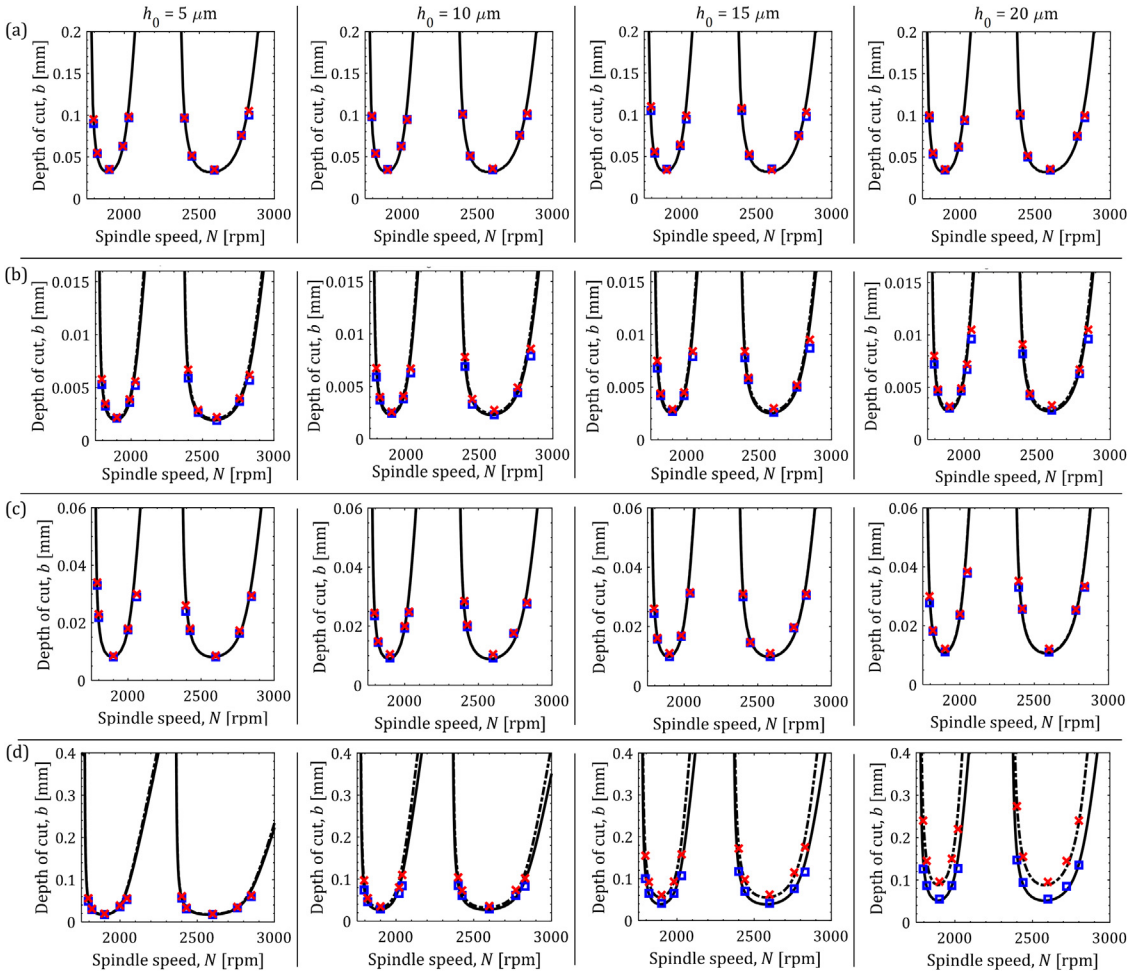

Fig. 5. Theoretical and emulated bistabilities for different forms of force models at four different levels of mean chip thickness. (a) linear (b) power-law, (c) cubic polynomial, (d) exponential. Theoretical global unstable and global stable curves are shown in dashed black and solid black lines respectively, and emulated global unstable and global stable results are shown with red cross and blue square markers respectively. (For interpretation of the references to colour in this figure legend, the reader is referred to the web version of this article).

case have been based on a time-delayed dynamic chip-thickness formulation leading to a linear or linearized DDE while the globally unstable limits from the HiL simulator have been obtained from the SLS algorithmic implementation for the total chip thickness. These two approaches are fundamentally different but a very good match between the stability boundaries obtained from the two approaches validates our implementation of the SLS algorithm for the estimation of the total chip thickness in the HiL simulator. This inspires confidence in the nonlinear results obtained on the simulator. Also comforting is the fact that stability investigations on the HiL simulator are based on a forward Euler numerical integration scheme and that the theoretical investigations are based on the semi-discretization method, and that both schemes, though different, give the same results. Since coefficients for all the linear and nonlinear models are different and are borrowed from different sources that were interested in characterizing force behavior for different materials of interest therein, results in Fig. 5 for the different force models should not be compared with each other.

For the linear case (Fig. 5(a)), the global unstable limit being independent of the mean static chip thickness (feed) is evident. And, for each of the nonlinear force models (Fig. 5(b–d)), the global unstable limit increasing with feeds is also evident. It is also clear that this increase is most dramatic for the case of the exponential force model (Fig. 5(d)). These results also suggest that if the process is to be stabilized, increasing the feed in some cases may help. This was also reported in Ref. [4] and is also an open secret amongst practicing engineers. And even though these observations are counterintuitive, they have practical significance.

Also evident from Fig. 5(b–d) is that for the feed range of interest, bistable regions for the power-law (Fig. 5(b)) and the cubic force model (Fig. 5(c)) do not change much, and that the correlation between the size of the bistable region and the feed is strongest for the case of the exponential force model (Fig. 5(d)). Also evident from Fig. 5, and in particular from Fig. 5(c), is how bistabilities are independent of speed. These observations are consistent with findings reported in Refs. [6,8]. A summary of emulated bistable regions changing with feed for different force models is shown in Fig. 6.

As is evident from Fig. 6, except for the low-feed region for the case of the cubic force model, emulations agree with theoretical predictions. These results have significance from the practical point of view in the sense that for exponential force models, since the size of the bistable regions increase with feed, more care needs to be exercised in selection of cutting parameters to lie outside such conditionally (un)stable regions. Results in Figs. 5 and 6 are also significant in the sense that, since the size of the bistable regions, and the minimum global unstable limit, both increase with an increase in the uncut chip thickness, and if cutting is desired to be carried out in regions that exhibit bistabilities with processes prone to strong perturbations, there is a very real case to explore active damping solutions to stabilize processes that are otherwise unstable and/or conditionally stable.

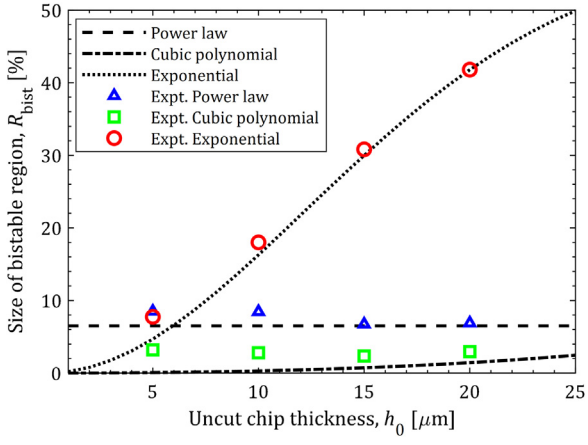

Fig. 6. Bistabilities changing with uncut chip thickness for different force models.

Gain tuning for active damping with nonlinear force characteristics and in the presence of bistabilities

Active control of vibrations is illustrated herein to demonstrate stable cutting in the otherwise bistable regions, or in regions that were otherwise globally unstable. We implement a direct velocity feedback control law in which the measured velocity ($\dot{x}(t)$) multiplied by a gain (K_{dvf} (Ns/m)) results in a damping force, $F_{act}(t) = -K_{dvf}\dot{x}(t)$, that increases with the gain. To characterize the dependence of gains on the force model and on the uncut chip thickness of interest, experiments were conducted to find the gains necessary to meet targeted improvement in the depths of cut at the speed and feeds (h_0) of interest. Separate experiments were undertaken for each of the linear and nonlinear force models. These results are summarized in Fig. 7. Separate experiments were also undertaken to investigate active damping in the presence of strong bistabilities, and those results are shown in Fig. 8.

For each force model of interest, gains were sought to meet three different levels of targeted improvements in the stable depths of cut at each of the four feeds of interest. Checks for gains required to meet three different targeted improvements in the depths of cut are to also investigate if gain requirements are (non) linearly proportional to the targeted improvement in the presence of nonlinearities in the force characteristics. For the linear case, since the global unstable limit (see Fig. 5(a)) is $\sim$32 μm, gains necessary to meet targeted depths of cut of $\sim$ 100 μm, $\sim$ 140 μm, and $\sim$ 180 μm were sought to be found. For the case of the power-law model, since the global unstable limit is weakly dependent on the feed, and is highest at $\sim$ 3 μm for the feed of 20 μm (see Fig. 5(b)), the gains necessary to meet targeted depths of cut of $\sim$ 5 μm, $\sim$ 10 μm, and $\sim$ 15 μm were sought to be found at every feed of interest. For the case of the cubic form of the force model, since the global unstable limit is also weakly dependent on the feed, and is highest at $\sim$ 10 μm for the feed of 20 μm (see Fig. 5(c)), the gains necessary to meet targeted depths of cut of $\sim$ 30 μm, $\sim$ 40 μm, and $\sim$ 50 μm were sought to be found at every feed of interest. And, finally, for the case of the exponential form of the force model, since the global unstable limit strongly dependent on the feed, and is highest at $\sim$90 μm for the feed of 20 μm (see Fig. 5(d)), the gains necessary to meet targeted depths of cut of $\sim$ 100 μm, $\sim$ 150 μm, and $\sim$ 200 μm were sought to be found at every feed of interest.

Experiments on the HiL simulator were conducted by turning the active controller 'On', and by tuning gains in the vicinity of model-based gain recommendations until the targeted improvement in the depth of cut was achieved. Turning the controller 'On' supplies a voltage to the secondary shaker which applies a force on the flexure to counter the large amplitude vibrations that were otherwise caused due to instabilities. For every speed, feed, depth of cut, and gain level, experimental procedures to establish stable/unstable cuts remained the same as those outlined in Fig. 4. Experimental results thus obtained are compared in Fig. 7 along with theoretical model-based results.

To realize active damping theoretically, the governing equation of motion from Eq. (1) is modified by adding the damping force to make it:

$$\ddot{x}(t) + 2\zeta\omega_n\dot{x}(t) + \omega_n^2 x(t) = \frac{1}{m}(F_f(t) + F_{act}(t)). \quad (20)$$

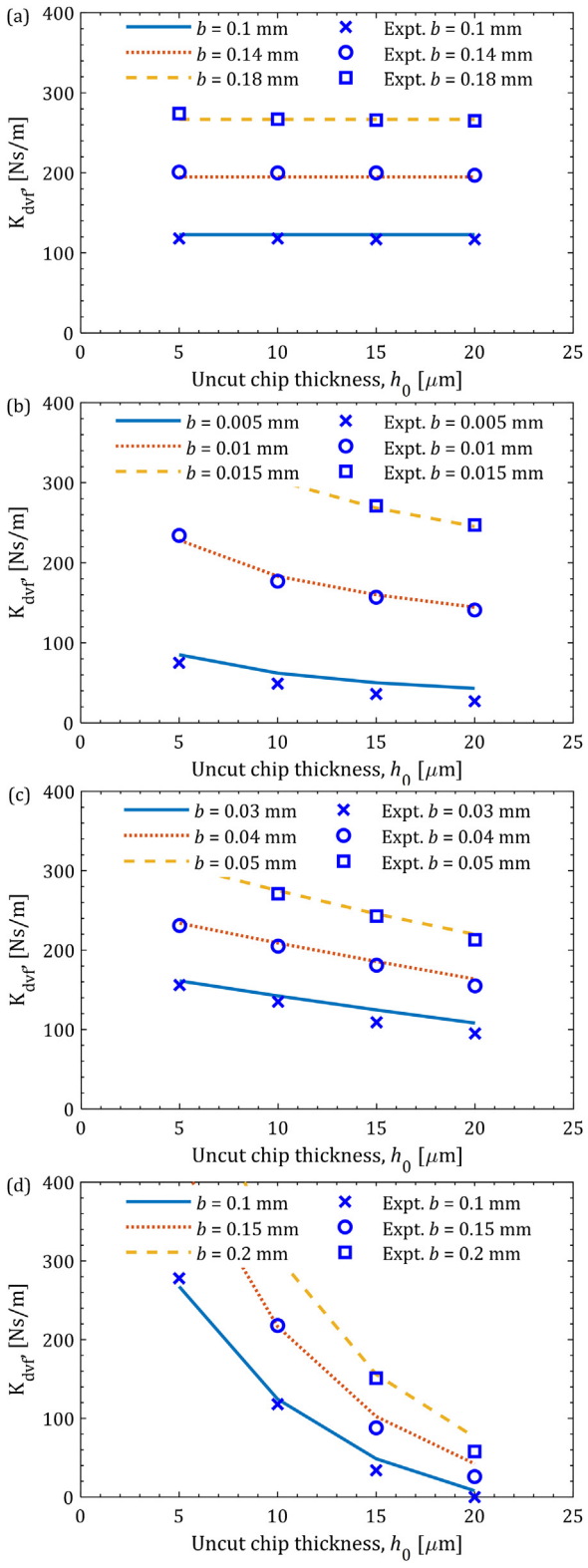

Fig. 7. Gains of the active damper changing with the force model and the uncut chip thickness of interest for three different levels of targeted improvement in the stable depth of cut at a speed of 2600 rpm. Experimental data points are overlaid on theoretical model-based findings (continuous curves). (a) Linear for model. (b) Power law force model. (c) Cubic form of the force model, and (d) Exponential force model.

The linearized form of Eq. (20) is solved using the SDM, wherein the only change in an updated form of Eq. (12) is that the coefficient matrix will become: $\mathbf{A}(t) = \begin{bmatrix} 0 & 1 \\ -\left(\omega_n^2 + \frac{F_f}{m}\right) & -\left(2\zeta\omega_n + \frac{K_{dvf}}{m}\right) \end{bmatrix}$. Following this change, the method of solution proceeds as already described. When the controller is 'Off', $K_{dvf} = 0$, and the problem reduces to the form already described. To find the gains that will result in the targeted depth of cut being stable at the speed and feeds of interest, we check for stability using the SDM for different values of control gains: $K_{dvf} \in 0 : 10 : 1000$ Ns/m. This range of gains are stable from the control perspective. Control stability was separately checked using the classical root locus technique. Results obtained for the different force models are summarized in Fig. 7. Results in Fig. 7 are limited to a speed of 2600 rpm, i.e., the speed at which the depth of cut is minimum for all force models of interest.

From Fig. 7(a), it is evident that for the case of the linear force model, gain tuning to meet the targeted stable chatter-free depths of cut is independent of the uncut chip thickness. From Fig. 7(b–d), it is also evident that for each of the nonlinear force model, the gain necessary to meet the targeted stable depths of cut is strongly dependent on the uncut chip thickness, and that gains reduce with increasing uncut chip thickness. For the nonlinear force characteristics, since the global unstable limits increase with feed, the gain required to meet targeted stable depths of cut decreasing with feed is unsurprising. It is further evident from Fig. 7(b–d), that the gains required to meet three different targeted improvements in the depths of cut are not strictly linearly proportional to the targeted improvement in depths of cut in the presence of nonlinearities in the force characteristics.

Some experiments for the nonlinear force models for the case of the highest targeted improvements in the depths of cut at lower feeds and with higher control gains resulted in a higher frequency mode of the flexure becoming unstable. Even though the higher frequency mode is dynamically much stiffer than the lower-frequency mode of the flexure, we cannot completely explain yet why it becomes unstable for higher gains. We suspect that it has something to do with the nature of control. This phenomena needs further study and can be investigated in future follow-on research. Moreover, since the flexure is modelled as a single degree of freedom system and its higher frequency modes are ignored, our model cannot predict the higher frequency mode becoming unstable. As such, these experimental results are hence not shown in Fig. 7. However, despite some missing experimental data, it is evident that emulations on the HiL simulator agree with theoretical model-based results. Since gains are independent of feed for the case of the linear force model, results in Fig. 7 confirm that tuning that is based on a linear model will be inadequate to damp vibrations to meet the targeted improvements in processes with potential nonlinearities in their force characteristics.

Having illustrated how gain tuning depends on force model characteristics, we also illustrate active damping in the presence of strong bistabilities. We restrict our investigations to the case of the exponential force model – which exhibited strong bistable behavior for the uncut chip thickness of $h_0 = 20\,\mu$m. We targeted a ~350% improvement in the global unstable limit, and the gain was set accordingly to be $K_{dvf} = 210$ Ns/m. Procedures to emulate bistable behavior on the HiL simulator with the controller being 'On' were the same as the case for when the controller was 'Off'. Theoretical global unstable limits with the controller being 'On' were predicted using the modified form Eq. (12) with the

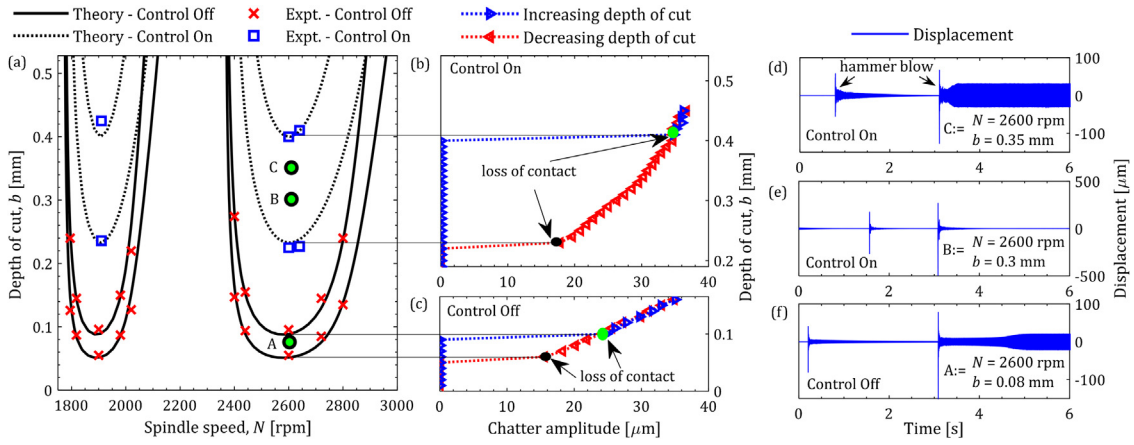

Fig. 8. (a) Theoretical and emulated bistabilities on the HiL simulator for the exponential force model at $h_0 = 20\,\mu$m in the control 'Off' and 'On' cases. (b) Experimental finite amplitude plot at 2600 rpm for the case of the control being 'On', (c) Experimental finite amplitude plot at 2600 rpm for the case of the control being 'Off', (d–e) Conditional stability check in the bistable region for the case of the control being 'On', (f) Conditional stability check in the bistable region for the case of the control being 'Off'. (For interpretation of the references to colour in this figure legend, the reader is referred to the web version of this article).

appropriate gain setting, and the theoretical global stable limit was predicted using Eqs. (14) and (17).

Experimentally characterized stability behavior is overlaid on theoretical predictions in Fig. 8(a) for the controller being 'Off' and 'On'. Fig. 8 also shows bistable behavior realized by generating finite amplitude instability plots for the specific spindle speed of 2600 rpm. These are shown for both cases of the controller being 'On' – Fig. 8(b), and for the controller being 'Off' – Fig. 8(c). Furthermore, to also verify characteristics of conditionally stable behavior, experiments were carried out by providing two levels of perturbations – one small, and another large. Perturbations were emulated by hammer blows on the flexure during emulated cutting at different parameters to understand the role of active damping in cutting processes prone to perturbations. Three depths of cut, i.e., point 'A', 'B', and 'C' shown in Fig. 8(a), were selected to check for conditional (in)stabilities. Point 'A' corresponds to 2600 rpm and $b = 0.08$ mm and lies within bistable region for the control being 'Off'. Point 'B' and 'C' corresponds to 2600 rpm and the depths of cut being $b = 0.3$ mm and $b = 0.35$ mm, respectively. And both these points lie within the bistable region for the case of the control being 'On'. Conditional check for (in)stabilities at these parameters is shown in Fig. 8(d–f).

From Fig. 8(a), it is evident that active damping can improve the global unstable limit as targeted. It is also evident that the emulated stability and bistability behavior emulated on the HiL simulator agrees well with model predictions. It is further evident that there exists a large bistable region even with the case of the controller being 'On', i.e., the bistable behavior retains its character since the force model remains nonlinear. Interestingly though the width of the bistable region appears larger with the control being 'On' than when it is 'Off', the larger width is attributable to the global unstable limit being higher (see Eqs. (14) and (17)), and is not an artefact of the active vibration control.

Bistability behavior is also evident from the plots for the finite amplitude instabilities shown in Fig. 8(b) and (c) — for the control being 'On' and 'Off', respectively. For both cases, the sudden jumps and drops in chatter amplitudes can be seen for a forward and backward sweep of the depth of cut. In both cases, the depths of cuts at which there is loss of contact of the tool with the workpiece are also highlighted. The green dot shows the global unstable point. And at this point, the first loss of contact of the tool with workpiece occurs. The black dot shows the second loss of contact which is encountered in the backward sweep of depth of cut.

The check for conditional stabilities for cutting at point 'A' within the bistable region for the control being 'Off' — shown in Fig. 8(f) confirms that for small perturbations the system remains stable, but for larger perturbations, the system becomes unstable. For the control being 'On', this point becomes globally stable. This demonstrates that regions that were conditionally and/or globally unstable for the control being 'Off' can become globally stable with the control being 'On'. For cutting at point 'B' which lies within the bistable region for the control being 'On', results of which are shown in Fig. 8(e), the cut remains stable for small and large perturbations due to the active damper stabilizing the cut, and due to the point 'B' lying closer to the global stable limit. Hence, point 'B' is also globally stable. And, finally, for cutting at point 'C' that lies within the bistable region for the control being 'On', results of which are shown in Fig. 8(d), the cut remains stable for small perturbations, and becomes unstable with larger ones, even when the controller in 'On'. This is attributable to the point 'C' lying closer to the global unstable limit. These results suggest that depending on the operating regime within the bistable region, the active damper may or not stabilize the cut in the presence of strong perturbations. Since the DVF control law implemented herein is linear, it cannot completely stabilize cutting in the bistable regime, and nor can it modify/eliminate the bistability.

Conclusions

This paper demonstrates the use of a hardware-in-the-loop simulator to emulate bistabilities in turning processes occurring due to nonlinear force characteristics. We also demonstrate active damping strategies to improve the globally unstable limit, and further show how active damping can stabilize cutting taking place in the bistable region even in the presence of strong disturbances. Since the size of the bistable region depends on the nonlinear form of the force, our investigations reveal that gains must be tuned for the force model and the static chip thickness under consideration, and that gain tuning using linear force models and stability analysis, as is usually done, is clearly inadequate.

All analysis presented herein is new, and demonstrates the utility of such emulations on a HiL simulator for it to instruct active damping strategies during more realistic cutting processes with nonlinear force characteristics that exhibit conditional instabilities in the presence of strong perturbations. The HiL simulator also presents the possibility of devising and testing nonlinear active

control laws to appropriately modify/eliminate bistable regions. Such investigations can further guide implementation on real machines. Furthermore, since the HiL simulator offers a safe, non-destructive and repeatable platform for such investigations, it makes possible emulations of many other such nuanced non-linearities (co)occurring in practice for a variety of machining processes to help devise solutions to mitigate them.

Declaration of interests

The authors declare that they have no known competing financial interests or personal relationships that could have appeared to influence the work reported in this paper.

Acknowledgments

This work was supported by theGovernment of India's Impacting Research Innovation and Technology (IMPRINT) initiative through project number IMPRINT 5509. We also acknowledge the anonymous reviewers for their probing and perceptive questions, addressing of which, has helped improve the manuscript.

References

[1] Tobias, S.A., Fishwick, W., 1958, Theory of Regenerative Machine Tool Chatter. The Engineer, 205/February (7): 199–203.
[2] Tlusty, J., Polacek, M., 1963, The Stability of the Machine Tool Against Self Excited Vibration in Machining. ASME Production Engineering Research Conference (Pittsburgh, PA, USA), pp.454–465.
[3] Tlusty, J., Ismail, F., 1981, Basic Non-linearity in Machining Chatter. CIRP Annals, 30/1: 299–304. http://dx.doi.org/10.1016/S0007-8506(07)60946-9.
[4] Shi, H.M., Tobias, S.A., 1984, Theory of Finite Amplitude Machine Tool Instability. International Journal of Machine Tool Design and Research, 24/1: 45–69. http://dx.doi.org/10.1016/0020-7357(84)90045-3.
[5] Nagy, K.T., Pratt, J.R., Davies, M.A., Kennedy, M.D., 1999, Experimental and Analytical Investigation of the Subcritical Instability in Metal Cutting. Proceedings of DETC'99 17th ASME Biennial Conference on Mechanical Vibration and Noise, 12–15.
[6] Dombovari, Z., Wilson, R.E., Stepan, G., 2008, Estimates of the Bistable Region in Metal Cutting. Proceedings of the Royal Society A: Mathematical Physical and Engineering Sciences, 464/2100: 3255–3271. http://dx.doi.org/10.1098/rspa.2008.0156.
[7] Stepan, G., Dombovari, Z., Munoa, J., 2011, Identification of Cutting Force Characteristics Based on Chatter Experiments. CIRP Annals, 60/1: 113–116. http://dx.doi.org/10.1016/j.cirp.2011.03.100.
[8] Molnar, T.G., Insperger, T., Stepan, G., 2018, Closed-form Estimations of the Bistable Region in Metal Cutting via the Method of Averaging. International Journal of Non-Linear Mechanics, 112:49–56. http://dx.doi.org/10.1016/j.ijnonlinmec.2018.09.005.
[9] Munoa, J., Mancisidor, I., Loix, N., Uriarte, L.G., Barcena, R., 2013, Chatter Suppression in Ram Type Travelling Column Milling Machines Using a Biaxial Inertial Actuator. CIRP Annals — Manufacturing Technology, 62:407–410. http://dx.doi.org/10.1016/j.cirp.2013.03.143.
[10] Ganguli, A., Deraemaeker, A., Horodinca, M.I., Preumont, A., 2005, Active Damping of Chatter in Machine Tools-demonstration with a 'Hardware-in-the-Loop' Simulator. Proceedings of the Institution of Mechanical Engineers Part I: Journal of Systems and Control Engineering, 219/5: 359–369. http://dx.doi.org/10.1243/095965105X33455.
[11] Ganguli, A., Deraemaeker, A., Romanescu, I., Horodinca, M.I., Preumont, A., 2006, Simulation and Active Control of Chatter in Milling via a Mechatronic Simulator. Journal of Vibration and Control, 12/8: 817–848. http://dx.doi.org/10.1177/1077546306064708.
[12] Kaliński, K.J., Galewski, M.A., 2014, Vibration Surveillance Supported by Hardware-in-the-Loop Simulation in Milling Flexible Workpieces. Mechatronics, 24/8: 1071–1082. http://dx.doi.org/10.1016/j.mechatronics.2014.06.006.
[13] Mancisidor, I., Beudaert, X., Etxebarria, A., Barcena, R., Munoa, J., Jugo, J., 2015, Hardware-in-the-Loop Simulator for Stability Study in Orthogonal Cutting. Control Engineering Practice, 44:31–44. http://dx.doi.org/10.1016/j.conengprac.2015.07.006.
[14] Sahu, G.N., Vashisht, S., Wahi, P., Law, M., 2020, Validation of a Hardware-in-the-Loop Simulator for Investigating and Actively Damping Regenerative Chatter in Orthogonal Cutting. CIRP Journal of Manufacturing Science and Technology, 115–129. http://dx.doi.org/10.1016/j.cirpj.2020.03.002.
[15] Mancisidor, I., Pena-Sevillano, A., Dombovari, Z., Barcena, R., Munoa, J., 2019, Delayed Feedback Control for Chatter Suppression in Turning Machines. Mechatronics, 63102276. http://dx.doi.org/10.1016/j.mechatronics.2019.102276.
[16] Matsubara, A., Tsujimoto, S., Kono, D., 2015, Evaluation of Dynamic Stiffness of Machine Tool Spindle by Non-contact Excitation Tests. CIRP Annals, 64/January (1): 365–368. http://dx.doi.org/10.1016/j.cirp.2015.04.101.
[17] Miklós, A., Bachrathy, D., Wohlfart, R., Takács, D., Porempovics, G., Tóth, A., Stépán, G.. 2018, Hardware-in-the-Loop Experiment of Turning, 77. p. pp.675–678. http://dx.doi.org/10.1016/j.procir.2018.08.179.
[18] Stepan, G., Beri, B., Miklos, A., Wohlfart, R., Bachrathy, D., Porempovics, G., Toth, A., Takacs, D., 2019, On Stability of Emulated Turning Processes in HIL Environment. CIRP Annals, 68/1: 405–408. http://dx.doi.org/10.1016/j.cirp.2019.04.035.
[19] Beri, B., Miklos, A., Takacs, D., Stepan, G., 2020, Nonlinearities of Hardware-in-the-Loop Environment Affecting Turning Process Emulation. International Journal of Machine Tools and Manufacture, 157:103611. http://dx.doi.org/10.1016/j.ijmachtools.2020.103611.
[20] Sahu, G.N., Vashisht, S., Jain. Wahi, P.P., Law, M., 2019, Investigating Nonlinear Finite Amplitude Chatter Instabilities Using a Hardware-in-the-Loop Simulator. 10th Int Cong On Mach (UTIS (Antalya, Turkey)), pp.15–21.
[21] Kienzle, O., 1952, Die Bestimmung von Kräften und Leistungen an spanenden Werkeugen und Werkzeugmaschinen, vol. 94. . VDI Z, 11/12.
[22] Endres, W.J., Loo, M., 2002, Modeling Cutting Process Nonlinearity for Stability Analysis—Application to Tooling Selection for Valve-seat Machining. Proc. 5th CIRP Workshop (International Workshop on Modeling of Machining Operation, West Lafayette, USA), .
[23] Insperger, T., Stépán, G., 2004, Updated Semi-discretization Method for Periodic Delay-differential Equations with Discrete Delay. International Journal for Numerical Methods in Engineering, 61/1: 117–141. http://dx.doi.org/10.1002/nme.1061.
[24] Batzer, S.A., Gouskov, A.M., Voronov, S.A., 2001, Modeling Vibratory Drilling Dynamics. ASME Journal of Vibration and Acoustic, 123/4: 435–443. http://dx.doi.org/10.1115/1.1387024.
[25] Wahi, P., Chatterjee, A., 2008, Self-Interrupted Regenerative Metal Cutting in Turning. International Journal of Non-linear Mechanics, 43/2: 111–123. http://dx.doi.org/10.1016/j.ijnonlinmec.2007.10.010.
[26] Dombovari, Z., Barton, D.A., Wilson, R.E., Stepan, G., 2011, On the Global Dynamics of Chatter in the Orthogonal Cutting Model. International Journal of Non-linear Mechanics, 46/1: 330–338. http://dx.doi.org/10.1016/j.ijnonlinmec.2010.09.016.
[27] Gupta, S.K., Wahi, P., 2016, Global Axial-torsional Dynamics During Rotary Drilling. Journal of Sound and Vibration, 375:332–352. http://dx.doi.org/10.1016/j.jsv.2016.04.021.
[28] Munoa, J., Zatarain, M., Bediaga, I., Peigne, G., 2006, Stability Study of the Milling Process Using an Exponential Force Model in Frequency Domain. HPC 2006 CIRP—2nd International Conference High Performance Cutting, Vancouver, Canada.
[29] Insperger, T., Stépán, G., Bayly, P.V., Mann, B.P., 2003, Multiple Chatter Frequencies in Milling Processes. Journal of Sound and Vibration, 262/2: 333–345. http://dx.doi.org/10.1016/S0022-460X(02)01131-8.
[30] Stepan, G., Hajdu, D., Iglesias, A., Takacs, D., Dombovari, Z., 2018, Ultimate Capability of Variable Pitch Milling Cutters. CIRP Annals, 67/1: 373–376. http://dx.doi.org/10.1016/j.cirp.2018.03.005.
[31] Schmitz, T.L., Smith, K.S., 2019, Machining Dynamics. Springer International Publishing. http://dx.doi.org/10.1007/978-3-319-93707-6.